Numerical Heat Transfer, Part A, 45: 517–538, 2004

ISSN: 1040-7782 print/1521-0634 online
DOI: 10.1080/10407780490277644

NUMERICAL DESIGN OF EFFICIENT SLOTTED FIN SURFACE BASED ON THE FIELD SYNERGY PRINCIPLE

Y. P. Cheng, Z. G. Qu, W. Q. Tao, and Y. L. He
State Key Laboratory of Multiphase Flow in Power Engineering,
School of Energy & Power Engineering,
Xi'an Jiaotong University, Xi'an, China

In this article, a numerical investigation of the flow and heat transfer in a three-row finned-tube heat exchanger is conducted with a three-dimensional laminar conjugated model. Four types of fin surfaces are studied; one is the whole plain plate fin, and the other three are of slotted type, called slit 1, slit 2, and slit 3. All four fin surfaces have the same global geometry dimensions. The three slotted fin surfaces have the same numbers of strips, which protrude upward and downward alternatively and are positioned along the flow direction according to the rule of "front coarse and rear dense." The difference in the three slotted fins is in the degree of "coarse" and "dense" along the flow direction. Numerical results show that, compared to the plain plate fin, the three types of slotted fin all have very good heat transfer performance in that the percentage increase in heat transfer is higher than that in the friction factor. Among the three slotted fin surfaces, slit 1 behaves the best, followed by slit 2 and slit 3 in order. Within the Reynolds number range compared (from 2,100 to 13,500), the Nusselt number of slit 1 is about 112–48% higher than that of the plain plate fin surface under the identical pumping constraint. An analysis of the essence of heat transfer enhancement is conducted from the field synergy principle, which says that the reduction of the intersection angle between the velocity and the temperature gradient is the basic mechanism for enhancing convective heat transfer. It is found that for the three comparison constraints the domain-average synergy angle of slit 1 is always the smallest, while that of the plain plate fin is the largest, with slit 2 and slit 3 being somewhat in between. The results of the present study once again show the feasibility of the field synergy principle and are helpful to the development of new types of enhanced heat transfer surfaces.

INTRODUCTION

Plate fin-and-tube heat exchangers are widely used in various engineering fields, such as heating, ventilating, air conditioning, and refrigeration (HVAC&R), automobiles, and air intercoolers. It is an effective way to reduce the air-side thermal

Received 1 August 2003; accepted 6 September 2003.
This work was supported by the National Key Project of Fundamental R & D of China (Grant 2000026303) and the National Natural Science Foundation of China (Grants 50236010, 50276046 and RFDP 20030698015).
Address correspondence to W. Q. Tao, School of Energy & Power Engineering, State Key Laboratory of Multiphase Flow in Power Engineering, Xi'an Jiaotong University, Xi'an, 710049, China. E-mail: wqtao@mail.xjtu.edu.cn

NOMENCLATURE

A	heat transfer area, m^2
c_p	specific heat at constant pressure, kJ/kg K
D_c	outer tube diameter, m
f	friction factor
h	heat transfer coefficient, W/m^2 K
Int	integral, $-\int\int_v\int \rho c_p(\mathbf{U} \cdot \nabla T)\, dv$,W
L	fin depth in air flow direction, m
p	pressure, Pa
Δp	pressure drop, Pa
Re	Reynolds number
T	temperature, K
$\mathbf{U}$	velocity vector
u	velocity in x direction, m/s
v	velocity in y direction, m/s
w	velocity in z direction, m/s

Γ	diffusion coefficient (λ/c_p)
θ	local intersection angle, deg
$\bar{\theta}$	mean intersection angle, deg
λ	thermal conductivity W/m K
μ	dynamic viscosity, kg/m s
ρ	air density, kg/m^3

Subscripts

in	inlet
m	mean
max	maximum
min	minimum
out	outlet
w	wall

resistance, which often accounts for about 90% of the overall thermal resistance. In order to further enhance the heat transfer, a variety of plate-fin surfaces have been developed. Broadly speaking, there are three generations of plate-fin surfaces. The first generation is the plain plate-fin (Figure 1), which is basically a continuous plain sheet of metal attached to a set of regularly positioned tubes. The second generation is the corrugated plate-fin, such as the wavy fin surface, in which streamwise corrugated flow channels are formed by bending the base sheet. Slotted fin surfaces, including the louvered fin and the slotted fin surface with protruding strips, may be regarded as the third generation. A large number of investigations, both experimental and numerical, have been conducted for a variety of plate-fin surfaces. A

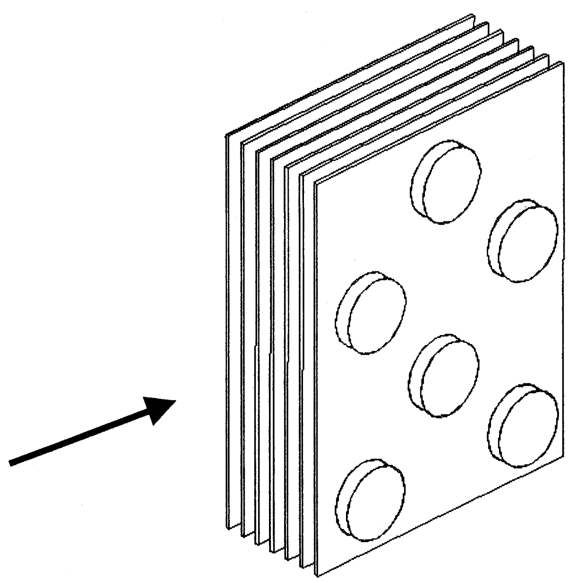

Figure 1. Schematic diagram of a fin-and-tube heat exchanger.

comprehensive review of numerical investigations on heat transfer and pressure drop characteristics of plate fin-and-tube heat exchangers published before 2000 has been performed by Shah et al. [1]. Very recent publications in this aspect include [2] for louvered fins, and [3, 4] for wavy fin surfaces. Recent experimental studies include [5–8]. Many studies have found that the louvered fin surface has very high heat transfer coefficient, but its pressure drop is sometime too high and prevents its wide applications. For example, Yun and Lee [9] used the scaled-up models in their experiment and compared the performance of plain fins, louvered fins, and three types of slotted fins, on which the slits cover the whole fin surfaces. The results showed that the slotted fins have greater j factors and smaller f factors than the louvered fins. In contrast, the slotted fin surfaces with protruding strips which are parallel to the base sheet have high heat transfer performance with acceptable pressure drop penalty, hence are widely adopted in engineering, especially in the air-conditioning and gas cooler industries. According to the comparison study of Kang et al. [10], under the identical pumping power constraint, among four kinds of plate-fin surfaces (plain, corrugated with a triangular-cross-sectional channel, corrugated with a sinusoidal-cross-sectional channel, and the slotted fin), the slotted fin surface behaves the best, and can increase heat transfer rate about 30–40% compared to the plain plate-fin. In this article, focus will be concentrated on the numerical design of efficient slotted fin surfaces.

The slotted fin was first studied by Nakayama and Xu [11]. They reported that its heat transfer coefficient can be 78% higher than that of the plain fin at 3-m/s air velocity. Later, Hiroaki et al. [12] provided experimental data for three kinds of strip position patterns having a high density of strips with an X-shape arrangement. They indicated that a heat exchanger with slotted fins can have one-third smaller volume than that with plain fins. Wang et al. [5, 6] made a systematic experimental investigation of slotted fin surfaces with strips protruding in one direction and in two directions alternatively along the flow direction, and provided experimental correlations of heat transfer and friction factor. Yun and Lee [7] analyzed the effects of various design parameters on the heat transfer and pressure drop characteristics of heat exchangers with slotted fins and presented the optimum value of each parameter.

The common feature of the slotted fin surfaces adopted in the above studies is that the slits are uniformly distributed along the streamwise direction. Recently, Kang and Kim [8] studied experimentally the effect of strip location on the heat transfer and pressure drop and found that the slotted fin with all the strips positioned in the rear part has better performance than that of a slotted fin with all the strips located in the front part. Qu et al. [13] validated numerically this interesting finding. They further applied the field synergy principle proposed by Guo et al. [14, 15] and enhanced in [16–19] to analyze these findings, and found the essence of the performance difference between the two kinds of slotted fins: the fin with rear strips has better synergy between velocity and the temperature gradient, i.e., less intersection angle between velocity and the temperature gradient.

From the traditional viewpoint, the reasons the interrupted geometries such as the slotted fin surface can enhance heat transfer are attributed to the decrease in the thermal boundary layer near the wall and/or the increase of the disturbance in the fluid. Recently, Guo and co-workers [14, 15] proposed a novel concept which is now called the field synergy principle for the boundary-layer flow. Its main idea is that reducing the intersection angle between the velocity and the temperature gradient is the basic mechanism for enhancing convective heat transfer. This idea was extended from parabolic flow to elliptic flow in [16], and numerical verifications were provided in [17] showing that the existing convective heat transfer enhancement mechanisms can be unified under the field synergy principle. A comprehensive review of recent studies of the field synergy principle is provided by Tao and He in [18, 19]. For the readers' convenience, the major idea of the field synergy principle is briefly reviewed as follows.

For a typical 2-D elliptical fluid flow and heat transfer over a backward step as shown in Figure 2, the steady-state governing equation of energy reads

$$\rho c_p\left(u\frac{\partial T}{\partial x}+v\frac{\partial T}{\partial y}\right)=\frac{\partial}{\partial x}\left(\Lambda\frac{\partial T}{\partial x}\right)+\frac{\partial}{\partial y}\left(\Lambda\frac{\partial T}{\partial y}\right) \tag{1}$$

Integrating this equation over the domain *abcdea*, we have $FM = HD$, where

$$FM=\iint_{\Omega=abcdea}\rho c_p(\mathbf{U}\cdot\nabla T)\,dx\,dy \tag{2a}$$

$$HD=\iint_{\Omega=abcdea}\left[\frac{\partial}{\partial x}\left(\Lambda\frac{\partial T}{\partial x}\right)+\frac{\partial}{\partial y}\left(\Lambda\frac{\partial T}{\partial y}\right)\right]dx\,dy \tag{2b}$$

By applying the Gauss theorem to reduce the integral dimensions, and moving the integrals along the inlet and outlet boundaries to the left-hand side, we obtain

$$\begin{aligned}\iint_{\Omega=abcdea}\rho c_p(\mathbf{U}\cdot\nabla T)\,dx\,dy-\int_{cd}\mathbf{n}\cdot\Lambda\nabla T\,dS-\int_{ea}\mathbf{n}\cdot\Lambda\nabla T\,dS\\=\int_{abc}\mathbf{n}\cdot\Lambda\nabla T\,dS+\int_{de}\mathbf{n}\cdot\Lambda\nabla T\,dS\end{aligned} \tag{3}$$

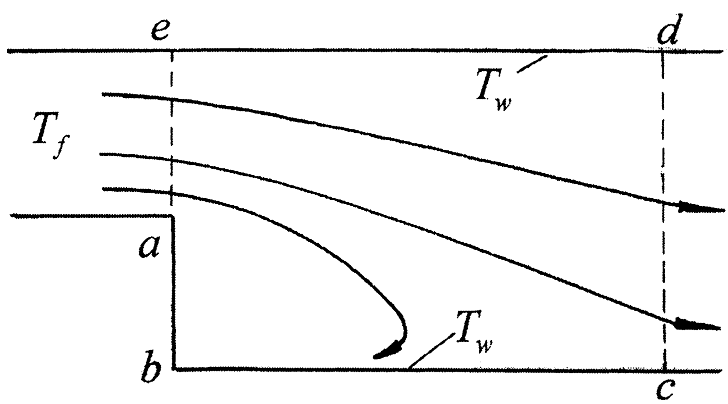

Figure 2. Fluid flow and heat transfer over a backward step.

The right-hand side of Eq. (3) stands for the convective heat transfer rate. The first term on the left-hand side is the energy transferred due to the fluid motion, while the second and the third terms stand for the axial heat conduction in the fluids. It is well known that for fluid flow with Peclet number larger than 100, the axial heat conduction within the fluid may be neglected compared to the energy transferred by the fluid motion [20]. Hence the integral $FM = \iint_{\Omega=abcdea} \rho c_p(\mathbf{U} \cdot \nabla T) dx\, dy$ represents the convective heat transfer rate. This term can be rewritten in the following form:

$$FM = \iint_{\Omega=abcdea} \rho c_P(\mathbf{U} \cdot \nabla T)\ dx\, dy = \iint_{\Omega=abcdea} \rho c_p |\mathbf{U}| \cdot |\nabla T| \cos\theta\, dx\, dy \tag{4}$$

From Eq. (4) it is clear that the smaller the intersection angle θ, the larger the heat transfer rate is under the same other conditions. In [17] it has been shown numerically that the existing three mechanisms for enhancing convective heat transfer actually lead to the reduction of this intersection angle. Thus it can be concluded that the most fundamental mechanism to enhance convective heat transfer is to reduce the intersection angle between the velocity and the temperature gradient, i.e., to make their synergy better. This is the major idea of the field synergy principle. For the convenience of discussion, this intersection angle is called the synergy angle hereafter.

The major purpose of the present study is to apply the field synergy principle to design an efficient slotted fin surface for use in gas intercoolers. It is required that the given number of strips should be appropriately located on the fin surface so that new slotted fin surface can enhance heat transfer by more than about 50% under the identical pumping power compared to an original plain plate fin surface within a wide range of oncoming flow velocity.

In the following presentation, the physical model and numerical formulation for the problem studied will first be presented, followed by detailed descriptions of the numerical treatment of the plain fin and slotted fin in the computation, and then numerical results will be provided. In this part, focus is first put on the reliability of the physical model and the code developed, and the results of mesh refinement study. Then the performance of three proposed slotted fins is quantitatively compared under different conditions, and their different performance is interpreted from the viewpoint of the field synergy principle. Finally, some conclusions will be drawn which are helpful in the design of new enhancement surfaces.

PHYSICAL MODEL

A schematic diagram of a typical plain-plate fin-and-tube heat exchanger used in an air intercooler is shown in Figure 1. There are three tube rows along the flow direction, which are arranged in a staggered way. Three types of slotted fin surfaces are proposed based on some preliminary computation and are shown in Figure 3, where the plain plate fin is also included for comparison purpose. The global geometries of the slotted fin surface are all the same as the plain plate fin. There are many pieces of strips in the slotted fin surfaces. The tube and fin are both made of copper. The air needed to be cooled flows along the fin surfaces and the cooling

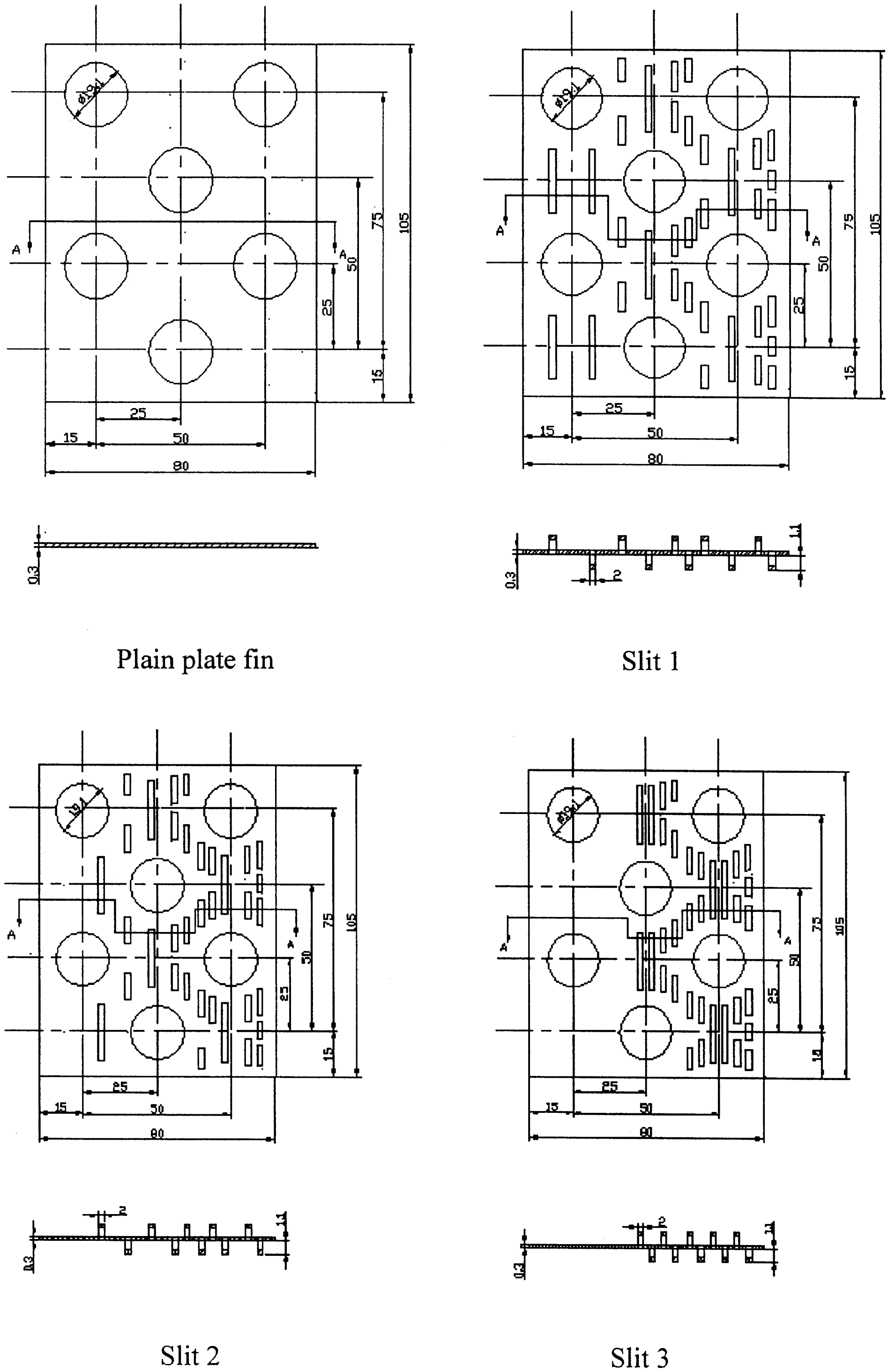

Figure 3. Geometry configuration of the four patterns of slit arrangement.

water goes through inside the tubes. The heat is transmitted from the air to the tube wall and the fin surface, then to the cooling water. The air is assumed to be incompressible with constant physical properties, and the flow is laminar and in a steady state. The heat transfer and pressure drop characteristics of the air side are to be solved by numerical modeling. Because of the relatively high heat transfer coefficient between the cooling water and the inner wall of the tube and the high thermal conductivity of the tube wall, the tube is assumed to be at constant temperature. However, temperature distribution in the fin surface is to be calculated, hence, the problem is of conjugated type in that both the temperature in the fin solid surface and in the fluid are to be determined simultaneously [21].

Figure 3 shows the details of geometry configurations of the four patterns of fins studied numerically in this article. In order to get a good heat transfer characteristic while avoiding a sharp increase of pressure drop, we first set a certain number of strips for the fin surface and then positioned them in different ways based on the findings in [8, 13]. Preliminary numerical simulations were then performed to find the ones which have better synergy between velocity and the temperature gradient, i.e., the average intersection angle between the velocity and the temperature gradient of the entire computational domain are smaller. Three types of strip arrangement were selected, which are presented in Figure 3. All three arrangements of strips possess the same feature: along the flow direction the distance between two neighboring strips gradually becomes smaller and smaller. Such a rule is simply called the rule of "front sparse and rear dense." All the strips of the three patterns protrude upward and downward alternatively along the flow direction, and each strip is punched with 2 mm width and 1.25 mm depth from the base chip. Numerical simulations are conducted for both plain fin and slotted fin surfaces under the same other conditions. The detailed geometries of the four heat exchanger surfaces simulated are presented in Table 1.

MATHEMATICAL FORMULATION

Computation Domain

According to the geometry characteristics of symmetry and period, the cell between two neighboring fin surfaces is investigated. Computational domain is shown in Figure 4 for a typical strip pattern of slit 1. In this figure, x is the

Table 1. Simulation conditions

Tube outside diameter	19.1 mm
Longitudinal tube pitch	25.0 mm
Transverse tube pitch	25.0 mm
Fin thickness	0.3 mm
Fin pitch	2.5 mm
Strip width	2.0 mm
Strip height	1.25 mm
Tube temperature	308 K
Inlet air temperature	403 K
Inlet frontal velocity	1.5--10.0 m/s

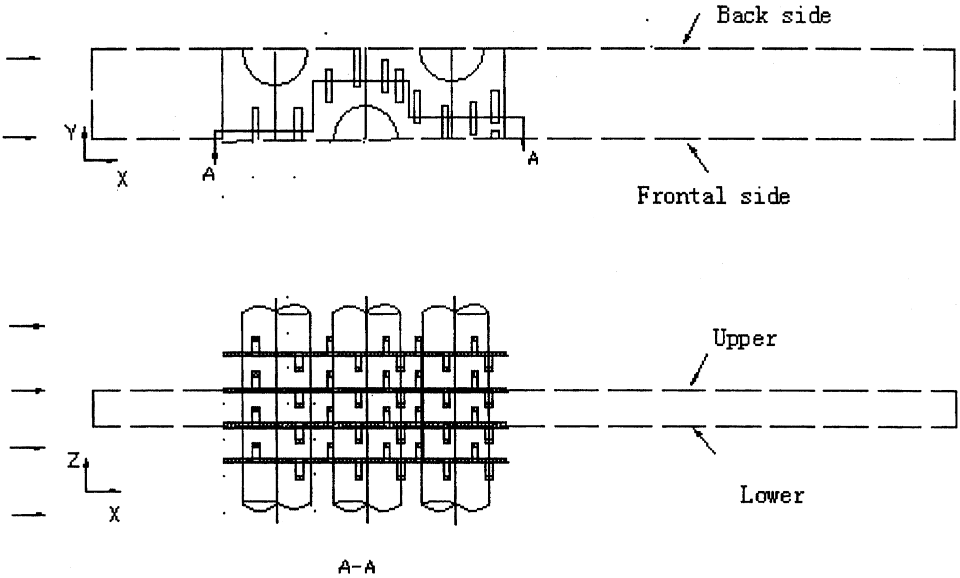

Figure 4. Computational domain of slit 1.

streamwise coordinate, y is the spanwise coordinate, and z stands for the fin pitch direction. The air flows across the fin surfaces from left to right. Because of the thickness of the fin, the air velocity profile is not uniform at the entrance to the channel formed by the fin surfaces. The computation domain is then extended upstream 1.5 times the streamwise fin length so that a uniform velocity distribution can be assigned at the domain inlet. The computational domain is extended downstream 10 times the streamwise fin length, so the one-way coordinate assumption can be adopted at the domain outlet [20, 21]. Thus the whole streamwise length of the computational domain is 12.5 times the actual fin length. To save space, the extended domain is not presented to scale in Figure 4. The dashed lines in Figure 4 show schematically such a computational domain in the x–y and z–x planes.

Governing Equations and Boundary Conditions

The governing equations for continuity, momentum, and energy in the computational domain can be expressed as follows.

Continuity equation:

$$\frac{\partial}{\partial x_i}(\rho u_i) = 0 \tag{5}$$

Momentum equations:

$$\frac{\partial}{\partial x_i}(\rho u_i u_k) = \frac{\partial}{\partial x_i}\left(\mu \frac{\partial u_k}{\partial x_i}\right) - \frac{\partial p}{\partial x_k} \tag{6}$$

Energy equation:

$$\frac{\partial}{\partial x_i}(\rho u_i T) = \frac{\partial}{\partial x_i}\left(\Gamma \frac{\partial T}{\partial x_i}\right) \tag{7}$$

where

$$\Gamma = \frac{\lambda}{c_p}$$

The governing equations are elliptic, hence boundary conditions are required for all boundaries of the computational domain. Due to the conjugated type of the problem, the fin surfaces are considered as a part of the solution domain and will be treated as a special type of fluid. The required conditions are described for the three regions as follows.

1. In the upstream extended region (domain inlet)

   At the inlet:

$$u = \text{const} \qquad T_{\text{in}} = \text{const} \qquad v = w = 0 \tag{8a}$$

   At the upper and lower boundaries:

$$\frac{\partial u}{\partial z} = \frac{\partial v}{\partial z} = 0 \qquad w = 0 \qquad \frac{\partial T}{\partial z} = 0 \tag{8b}$$

   At the front and back sides:

$$\frac{\partial u}{\partial y} = \frac{\partial w}{\partial y} = 0 \qquad v = 0 \qquad \frac{\partial T}{\partial y} = 0 \tag{8c}$$

2. In the downstream extended region (domain outlet)

   At the upper and lower boundaries:

$$\frac{\partial u}{\partial z} = \frac{\partial v}{\partial z} = 0 \qquad w = 0 \qquad \frac{\partial T}{\partial z} = 0 \tag{9a}$$

   At the front and back sides:

$$\frac{\partial u}{\partial y} = \frac{\partial w}{\partial y} = 0 \qquad v = 0 \qquad \frac{\partial T}{\partial y} = 0 \tag{9b}$$

   At the outlet boundary:

$$\frac{\partial u}{\partial x} = \frac{\partial v}{\partial x} = \frac{\partial w}{\partial x} = \frac{\partial T}{\partial x} = 0 \tag{9c}$$

3. In the fin coil region
   (*a*) For the plain plate fin

   At the upper and lower surfaces:

$$u = v = w = 0 \qquad \frac{\partial T}{\partial z} = 0 \tag{10a}$$

   At the front and back sides:

$$\text{Fluid region:} \qquad \frac{\partial u}{\partial y} = \frac{\partial w}{\partial y} = 0 \qquad v = 0 \qquad \frac{\partial T}{\partial y} = 0 \tag{10b}$$

$$\text{Fin surface region:} \qquad u = v = w = 0 \tag{10c}$$

$$\text{Tube region:} \qquad u = v = w = 0 \qquad T_w = \text{const} \tag{10d}$$

$$\text{Temperature condition for both fin and fluid regions}: \frac{\partial T}{\partial y} = 0 \tag{10e}$$

   (*b*) for the slotted fin

   At the upper and lower surfaces:

$$\text{Velocity at solid:} \qquad u = v = w = 0 \tag{11}$$

   Velocity of the fluid in the slits: periodic conditions

   Temperature for both solid and fluid: periodic conditions

The other conditions of the strip fin surface are the same as the plain plate fin.

Numerical Methods

The fluid–solid conjugated heat transfer problem is solved by the full-field computation method. The solid in the computational domain is regarded as a special fluid of infinite viscosity. The harmonic mean method is adopted for the interface diffusion coefficient. To guarantee the continuity of the flux rate at the interface, the thermal conductivity of the fin and fluid adopt individual values, while the heat capacity of the solid takes the value of the fluid (see Γ in Eq. (7) and Ref. [21]). To simulate the strip configuration, a special array called LAG is introduced to identify different regions: fluid, fin, and tube. The circular geometry of the tube is approximated by the stepwise method. A very large value of the thermal conductivity is assigned to the tube region to guarantee the tube temperature to be constant. The detailed computational method of conjugated heat transfer can be found in [22, 23]. The computational domain is discretized by nonuniform grids, with the grids of the fin coil region being fine, and those in the extension domains being coarse. The total grid points are $211 \times 85 \times 24$. Governing equations are discretized by the finite-volume method, and the convection term is discretized by the SGSD scheme [24]. The coupling between pressure and velocity is implemented by the CLEAR algorithm

[25, 26]. The convergence criterion for the velocities is that the maximum mass residual of the cells divided by the inlet mass flux is less than 5.0×10^{-6}, and the criterion for temperature is that the difference between two heat transfer rates obtained from an iteration and after successive 50 iterations is less than 1.0×10^{-6}.

RESULTS AND DISCUSSION

Parameter Definitions

Some parameters are defined as follows:

$$\mathrm{Re} = \frac{\rho u_m D_e}{\mu} \tag{12}$$

$$\mathrm{Nu} = \frac{h D_e}{\lambda} \tag{13}$$

$$h = \frac{Q}{A\,\Delta T} \tag{14}$$

$$Q = \dot{m} c_p (T_{\mathrm{in}} - T_{\mathrm{out}}) \tag{15}$$

$$\Delta p = p_{\mathrm{in}} - p_{\mathrm{out}} \tag{16}$$

$$f = \frac{\Delta p}{1/2 \rho u_m^2} \cdot \frac{D_e}{L} \tag{17}$$

$$j = \frac{\mathrm{Nu}}{\mathrm{Re}\,\mathrm{Pr}^{1/3}} \tag{18}$$

$$\Delta T = \frac{T_{\max} - T_{\min}}{\log\left(\frac{T_{\max}}{T_{\min}}\right)} \tag{19}$$

$$\theta = \arccos\left(\frac{\mathbf{U} \cdot \nabla T}{|\mathbf{U}||\nabla T|}\right) \tag{20}$$

$$\bar{\theta} = \frac{\iiint\limits_V \theta\, dv}{\iiint\limits_V dv} \tag{21}$$

$$\mathrm{Int} = -\iiint\limits_V \rho c_p (\mathbf{U} \bullet \nabla T)\, dv \tag{22}$$

where u_m is the mean velocity of the minimum transverse area, D_e is the outer tube diameter, T_{in}, T_{out} are the bulk temperatures of the inlet and outlet of the fin surface, respectively, and $T_{\max} = \max(T_{\mathrm{in}} - T_w, T_{\mathrm{out}} - T_w)$, $T_{\min} = \min(T_{\mathrm{in}} - T_w,\ T_{\mathrm{out}} - T_w)$.

It should be noted that for the case studied fluid is cooled and the integral $\iiint_V \rho c_p(\mathbf{U} \bullet \nabla T)\, dv$ is less than zero. For convenience of presentation, a minus sign is added in the definition of Int in Eq. (22). Further, when the local synergy angle is larger than 90°, it is replaced by $180 - \theta$ in the calculation of the average synergy angle by Eq. (21), for convenience of comparison discussion.

Validation of the Code and Mesh Independence of the Solution

To validate the computational model and the code developed, preliminary computations were first conducted for the plain-plate fin surface, and the predicted pressure drop and Nusselt number were compared with the experimental correlations provided by Wang et al. [27]. Their correlations were developed based on 74 samples of plain plate fins and can describe 85.1% of the database for pressure drop and 88.6% of the database for heat transfer, both within 15%. The variation range of the Reynolds number is from 2.0×10^2 to 2.0×10^4. These are the most accurate and reliable correlations with wide applicable ranges known to the present authors. The comparison results are provided in Figure 5: the maximum deviation in pressure drop is less than 6% and that of the Nusselt number is less than 10%. The good agreement between the predicted and tested results shows the reliability of the physical model and the code developed.

In order to adopt an appropriate grid system, a grid refinement was conducted to investigate the influence of the grid density on the computational results. Take the Nusselt number of slit 1 as example. The results of four different grid systems are shown in Figure 6. Compared to the finest grid $211 \times 127 \times 24$, the grid $211 \times 85 \times 24$ yields 0.8% lower Nu number. Thus, in order to save computer resources, the grid system $211 \times 85 \times 24$ was adopted in the other numerical simulation. The code validation was also conducted on this grid system.

Comparisons under the Identical Re Number

In Figure 7 we compare j factors of the four patterns of fins shown in Figure 3 under different Reynolds numbers ranging from 2.1×10^3 to 1.3×10^4 (the corresponding frontal velocities range from 1.5 to 10 m/s, which covers the working flow velocity for gas intercoolers). As expected, the three types of slotted fins (slit 1, slit 2, and slit 3) all have higher heat transfer performance than that of the plain plate fin. However, with the increase of the Reynolds number the enhancing function of strips gradually becomes less significant. For example, the j factor for slit 1 is one time higher than that of the plain plate fin at $\mathrm{Re} = 2.1 \times 10^3$, but only 60% at $\mathrm{Re} = 1.3 \times 10^4$. It is very exciting to note that, compared to the plain plate fin, the increase of f factor for these three slit fins is much less than that of j factor. In the whole range of Re number compared, the friction factor of slit 1 is only about 40% higher than that of the plain plate fin. It is also interesting to note that slit 1 always provides more heat transfer rate than slit 3. Within the range of Reynolds number studied, the values of j factor for slit 1 are about 9% higher than those of slit 3, with slit 2 being somewhat in between.

The predicted friction factors are presented in Figure 8. From the figure we can see that slit 1 has the lowest friction factors among the three slit fins. The ratio j/f,

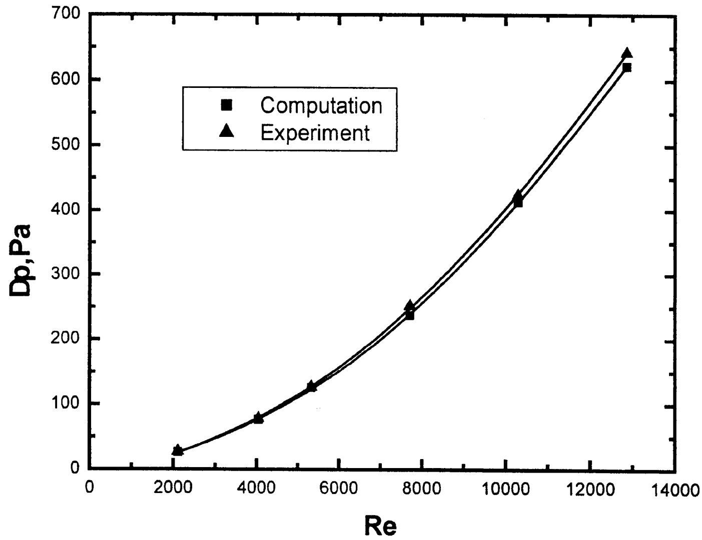

(a) Pressure drop

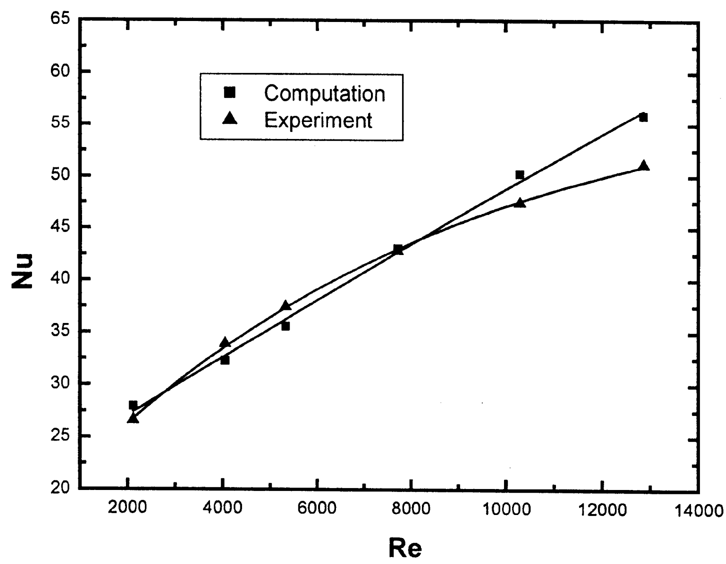

(b) Nusselt number

Figure 5. Comparison between predicted and test results.

which is an index in evaluating the fin surface proposed by Shah [28], is presented in Figure 9, where the superior performance of slit 1 can be clearly observed. Thus it is doubtless that slit 1 has the best comprehensive performance among the four types of fins. It is apparent that the increase of *f* factors for these three slotted fins is much

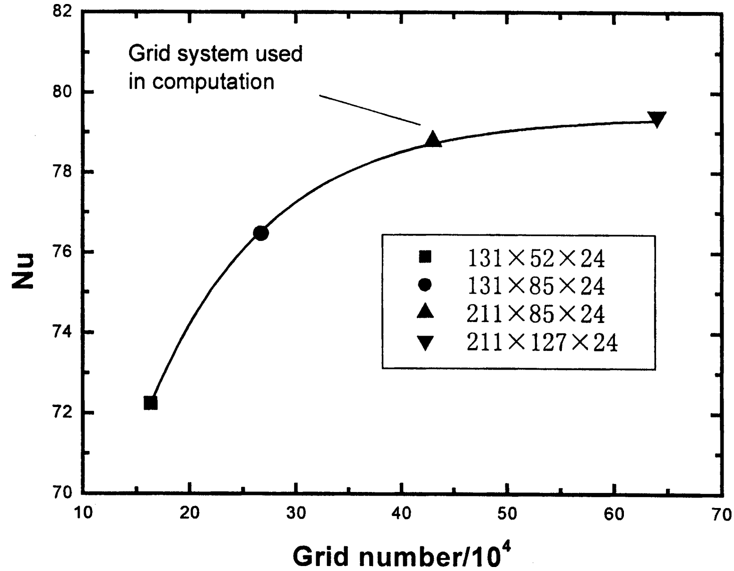

Figure 6. Nusselt number of slit 1 against the grid number.

less than that of the j factors. The excellent performance of slit 1 has also been verified in the multistage heat exchanger, which will be addressed in another article.

Comparison under the Identical Pressure Drop and Identical Pumping Power

In order to appraise the performance of four types of fin surfaces, comparisons are made under the other two constraints [29]: (1) identical pressure drop; and (2) identical pumping power. As the characteristic dimensions of the four types of fin surface are all the same, the following conditions must be met to satisfy these two constraints:
Identical pressure drop:

$$\left(f\mathrm{Re}^2\right)_{\mathrm{Plain}} = \left(f\mathrm{Re}^2\right)_{\mathrm{Slit1}} \tag{23a}$$

$$\left(f\mathrm{Re}^2\right)_{\mathrm{Slit2}} = \left(f\mathrm{Re}^2\right)_{\mathrm{Slit1}} \tag{23b}$$

$$\left(f\mathrm{Re}^2\right)_{\mathrm{Slit3}} = \left(f\mathrm{Re}^2\right)_{\mathrm{Slit1}} \tag{23c}$$

Identical pumping power

$$\left(f\mathrm{Re}^3\right)_{\mathrm{Plain}} = \left(f\mathrm{Re}^3\right)_{\mathrm{Slit1}} \tag{24a}$$

$$\left(f\mathrm{Re}^3\right)_{\mathrm{Slit2}} = \left(f\mathrm{Re}^3\right)_{\mathrm{Slit1}} \tag{24b}$$

$$\left(f\mathrm{Re}^3\right)_{\mathrm{Slit3}} = \left(f\mathrm{Re}^3\right)_{\mathrm{Slit1}} \tag{24c}$$

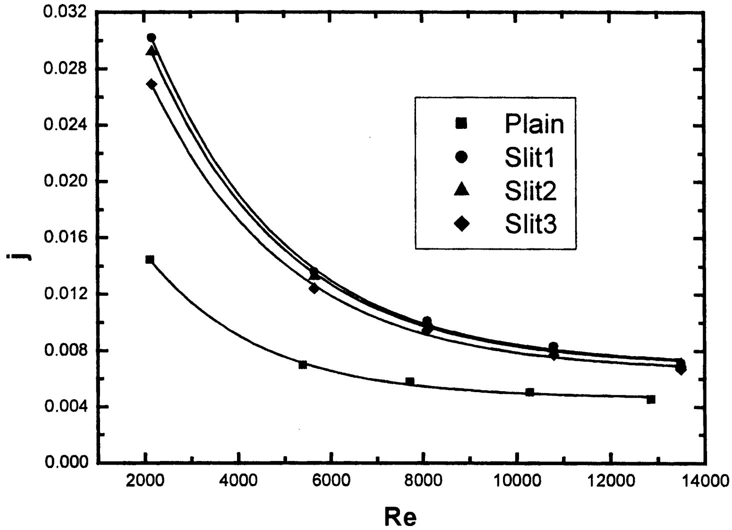

Figure 7. Computational results of j factor against Re number.

The evaluation proceeds in the following way. First, according to the computational results, the relations between f factor, Nusselt number, averaged synergy angle, and Reynolds number are obtained. Then select a Reynolds number for slit 1; the corresponding Reynolds numbers for the plain plate fin, slit 2, and slit 3 can be determined in an iterative manner from the relations of f versus Re and Nu versus Re. Taking the Re of slit 1 as the abscissa, the corresponding Reynolds number of

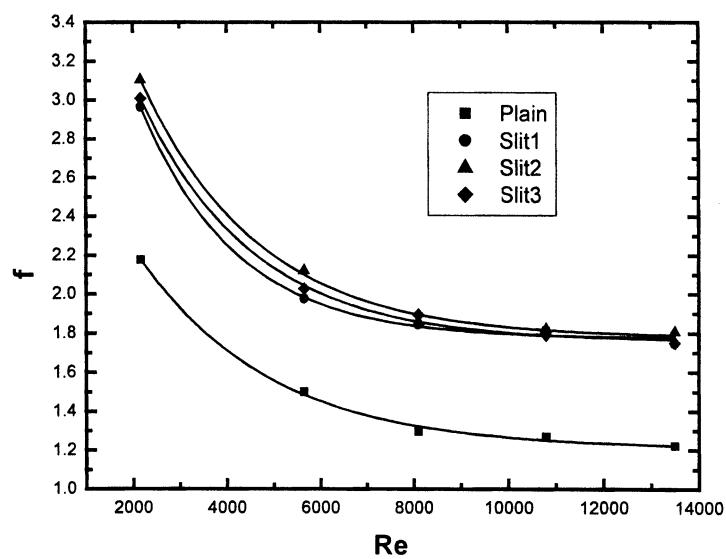

Figure 8. Computational results of f factor against Re number.

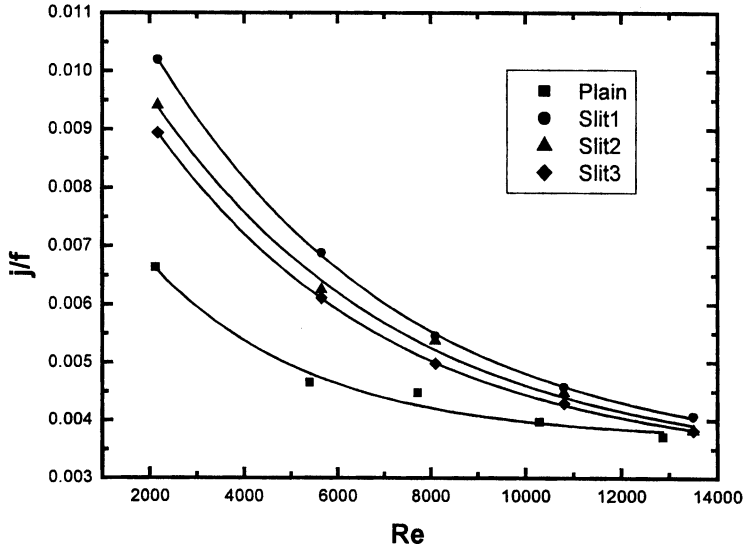

Figure 9. Computational results of j/f against Re number.

the other three cases can be found and, hence, the related Nusselt number. The values of Nu are plotted as the ordinates. The results are shown in Figures 10 and 11. It can be seen that under the two constraints adopted, slit 1 has the best performance, followed by slit 2, slit 3, and the plain plate fin in order. The heat transfer enhancement of slit 1 is very appreciable. For example, compared to the plain plate fin, under the identical pressure drop the increased percentage of Nu number ranges from 109% to 43%, and under the identical pumping power this percentage varies from 112% to 48%. Under the two constraints slit 1 always has an average 10% higher Nusselt number than that of slit 3, and slit 2 is always in between.

It is the point to reveal why slit 1 behaves best among the three slotted fin patterns compared. The field synergy principle can give us a satisfactory explanation.

DISCUSSION ON HEAT TRANSFER ENHANCEMENT ESSENCE

From the traditional viewpoint, strips on the fin surface can enhance convective heat transfer because they can interrupt the flow boundary layer to reduce the thermal boundary-layer thickness by repeatedly re-creating the thermal boundary layers, or can increase the disturbance in the flow field. As indicated above, all these functions come from the same source: the reduction of the synergy angle. The comparisons of the domain-averaged synergy angle of the four types of fin surface under different constraints are presented in Figures 12, 13, and 14. From these figures, the following features may be noted. First, the results show that the mean synergy angles increase with increase of Re number, which indicates that the synergy between velocity and the temperature gradient becomes worse with increasing Re.

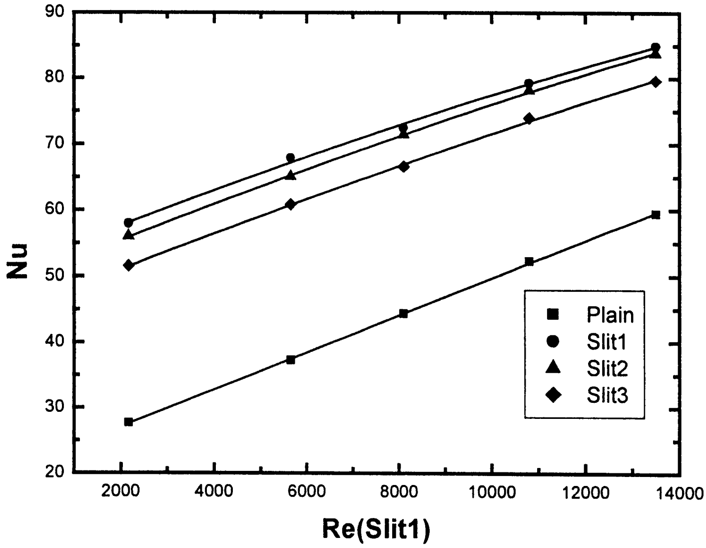

Figure 10. Comparison of Nu under identical pressure drop.

This can explain why with the increase in flow rate the convective heat transfer rate does not increase linearly, and the larger the Reynolds number, the less significant is the increase in heat transfer (see Figure 15). Second, under any conditions compared, the three slotted fins always have lower averaged synergy angle than that of the plain plate fin. Although the absolute difference of the synergy angle for the cases studied

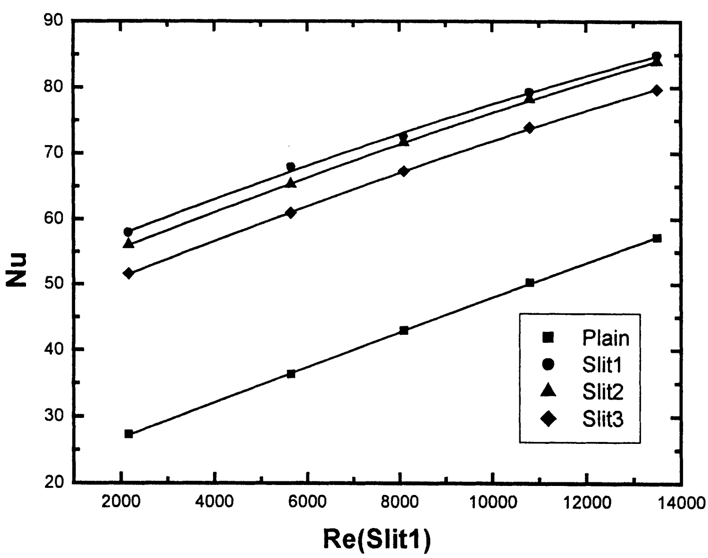

Figure 11. Comparison of Nu under identical pumping power.

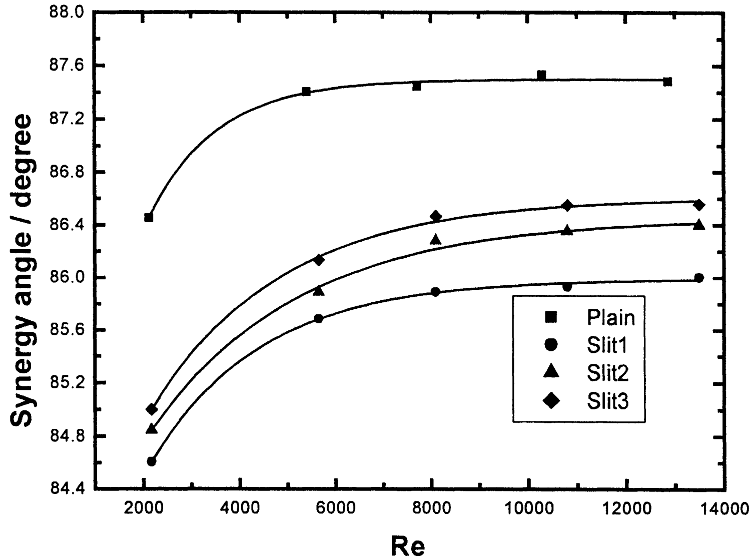

Figure 12. Comparison of domain-averaged synergy angle against Re number.

is less than 2°, this will lead to a difference in cosine of more than 30% (for example, the cosine of 84.8° is 0.09063, while the cosine of 86.6° is 0.05931). Thus we can conclude that the function of strips on the slotted fin surface is to improve the synergy between the velocity and the temperature gradient. Third, it is especially

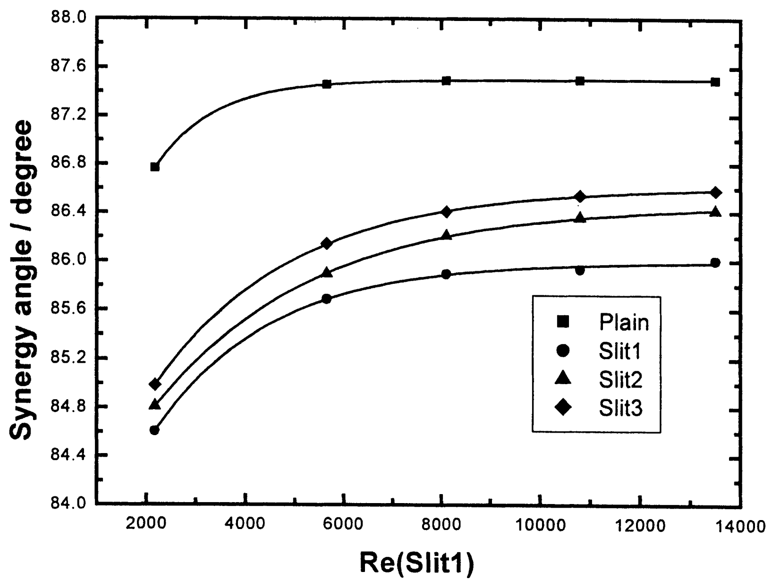

Figure 13. Comparison of domain-averaged synergy angle under identical pressure drop.

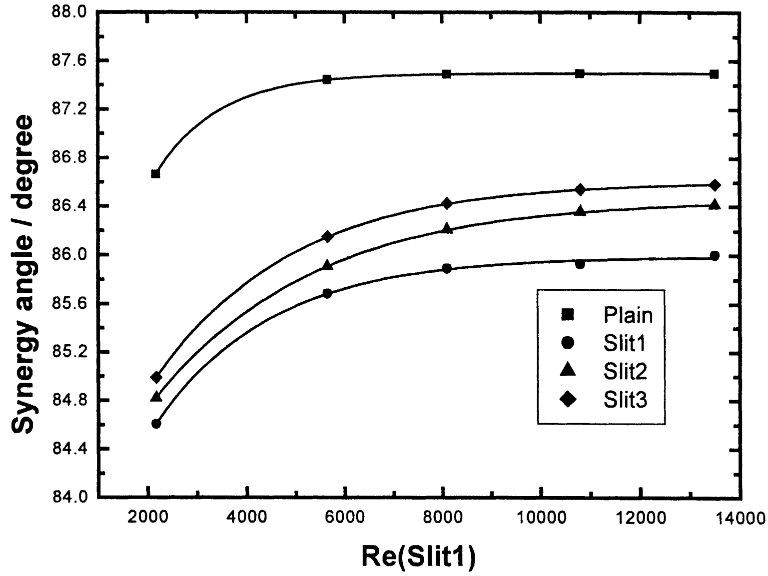

Figure 14. Comparison of domain-averaged synergy angle under identical pumping power.

interesting to note that the averaged synergy angle of slit 1 is always lower than that of the other two slit fins. This is the most fundamental reason why slit 1 has the best performance among the four fins compared.

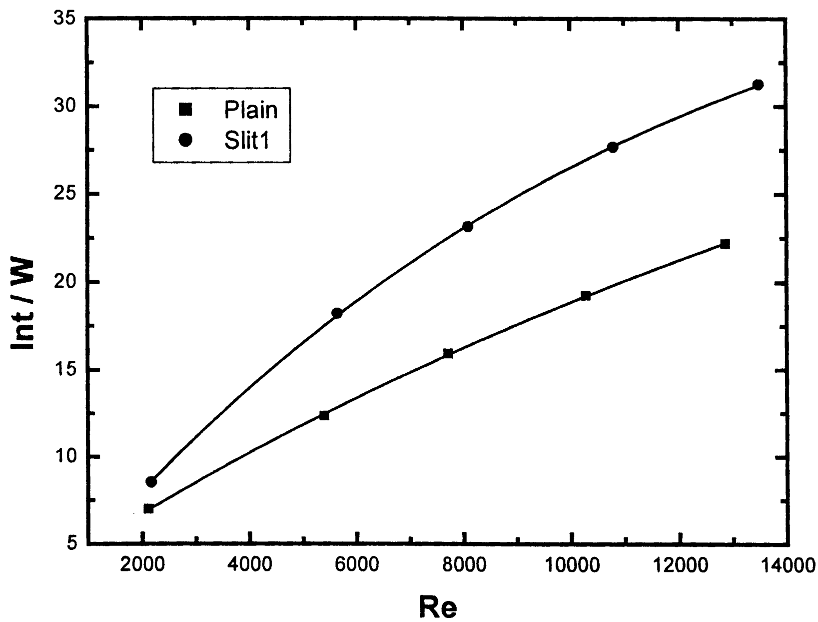

Figure 15. Integral of slit 1 and plain plate fin against Re number.

CONCLUSIONS

In this article, the air-side heat transfer and pressure drop of three types of slotted fin and a plain plate fin are performed using a three-dimensional steady laminar model within the Re number range from 2.1×10^3 to 1.3×10^{-4}. The predicted results of heat transfer and friction factor for the plain plate fin agree well with the tested data available in the literature. The numerical results are analyzed with the field synergy principle. The major findings are summarized as follows.

1. Three types of slotted fin surfaces are proposed in which the strips are distributed along the flow direction according the rule of "front sparse and rear dense." Compared to the plain plate fin, the three types of slit fin all have very good heat transfer performance in that the percentage increase in heat transfer is higher than that in the friction factor. Within the Reynolds number range studied, the j factor of the slotted fin is at least 40–86% higher than that of the plain plate fin, while the increase in the friction factor ranges only from 36% to 50%.
2. The performance of the three slotted fins and the plain plate fin are compared under three constraints: identical mass flow rate, identical pressure drop, and identical pumping power. The comparison results are quite consistent in that slit 1 always has the best performance, followed by slit 2 and slit 3, and the plain plate fin, in order.
3. An analysis for the four types of fin surfaces is carried out with the field synergy principle and the domain-averaged synergy angles are calculated under the three comparison constraints. The results show that the significant difference in the heat transfer performance comes from the different synergy levels between velocity and the temperature gradient. The synergy angle of slit 1 is the smallest, and that of the plain plate fin is the largest, with slit 2 and slit 3 being in between.
4. The numerical results of the present study once again demonstrate that the field synergy principle proposed by Guo et al. reveals the fundamental mechanism for enhancing convective heat transfer and is a very useful tool in developing new types of enhanced heat transfer structure.

REFERENCES

1. R. K. Shah, M. R. Heikal, B. Thonon, and P. Tochon, Progress in the Numerical Analysis of Compact Heat Exchanger Surfaces, *Adv. Heat Transfer*, vol. 34, pp. 363–442, 2000.
2. J. S. Leu, M. S. Liu, J. S. Liaw, and J. S. Wang, A Numerical Investigation of Louvered Fin-and-Tube Heat Exchangers Having Circular and Oval Tube Configuration, *Int. J. Heat Mass Transfer*, vol. 44, pp. 4235–4243, 2001.
3. J. C. Min and R. L. Webb, Numerical Prediction of Wavy Fin Coil Performance, *Enhanced Heat Transfer*, vol. 8, pp. 159–173, 2001.
4. G. Comini and G. Croce, Convective Heat and Mass Transfer in Tube-Fin Exchangers under Dehumidifying Conditions, *Numer. Heat Transfer A*, vol. 40, pp. 579–599, 2001.
5. C. C. Wang, W. H. Tao, and C. J. Chang, An Investigation of the Air Side Performance of the Slit Fin-and-Tube Heat Exchangers, *Int. J. Refrig.*, vol. 22, pp. 595–603, 1999.

6. Y. J. Du and C. C. Wang, An Experimental Study of the Airside Performance of the Superslit Fin-and-Tube Heat Exchangers, *Int. J. Heat Mass Transfer*, vol. 43, pp. 4475–4482, 2000.
7. J. Y. Yun and K. S. Lee, Influence of Design Parameters on the Heat Transfer and Flow Friction Characteristics of the Heat Exchanger with Slit Fins, *Int. J. Heat Mass Transfer*, vol. 43, pp. 2529–2539, 2000.
8. H. C. Kang and M. H. Kim, Effect of Strip Location on the Air-Side Pressure Drop and Heat Transfer in Strip Fin-and-Tube Heat Exchanger, *Int. J. Refrig.*, vol. 22, pp. 302–312, 1998.
9. J. Y. Yun and K. S. Lee, Investigation of Heat Transfer Characteristics on Various Kinds of Fin-and-Tube Heat Exchangers with Interrupted Surfaces, *Int. J. Heat Mass Transfer*, vol. 42, pp. 2375–2385, 1999.
10. H. J. Kang, W. Li, H. J. Li, R. C. Xin and W. Q. Tao, Experimental Study on Heat Transfer and Pressure Drop Characteristics of Four Types of Plate Fin-and-Tube Heat Exchanger Surfaces, *Int. J. Thermal Fluid Sci.*, vol. 3, no. 1, pp. 34–42, 1994.
11. W. Nakayama and L. P. Xu, Enhanced Fins for Air-Cooled Heat Exchangers—Heat Transfer and Friction Factor Corrections, *Proc. 1983 ASME-JSME Thermal Eng. Conf.*, vol. 1, pp. 495–502, 1983.
12. K. Hiroaki, I. Shinichi, A. Osamu, and K. Osao, High-Efficiency Heat Exchanger, *Natl. Tech. Rep.*, vol. 35, no. 6, pp. 653–661, 1989.
13. Z. G. Qu, W. Q. Tao, and Y. L. He, 3D Numerical Simulation on Laminar Heat Transfer and Fluid Flow Characteristics of Slitted Fin Surface: Investigation of Strip Location Effects, In R. K. Shah et al. (eds), *Compact Heat Exchangers and Enhancement Technology for the Process Industries-2003*, pp. 9–16, Begell House, New York, 2003.
14. Z. Y. Guo, D. Y. Li, and B. X. Wang, A Novel Concept for Convective Heat Transfer Enhancement, *Int. J. Heat Mass Transfer*, vol. 41, pp. 2221–2225, 1998.
15. S. Wang, Z. X. Li, and Z. Y. Guo, Novel Concept and Devices of Heat Transfer Augmentation, *Proc. 11th Int. Conf. Heat Transfer*, vol. 5, pp. 405–408, 1998.
16. W. Q. Tao, Z. Y. Guo, and B. X. Wang, Field Synergy Principle for Enhancing Convective Heat Transfer—Its Extension and Numerical Verifications, *Int. J. Heat Mass Transfer*, vol. 45, pp. 3849–3856, 2002.
17. W. Q. Tao, Y. L. He, Q. W. Wang, Z. G. Qu, and F. Q. Song, A Unified Analysis on Enhancing Convective Heat Transfer with Field Synergy Principle, *Int. J. Heat Mass Transfer*, vol. 45, pp. 4871–4879, 2002.
18. W. Q. Tao and Y. L. He, Field Synergy Principle and Its Applications in Enhancing Convective Heat Transfer and Improving Performance of Pulse Tube Refrigerators (Part 1), *J. Xi'an Jiaotong Univ.*, vol. 36, no. 11, pp. 1101–1105, 2002.
19. Y. L. He and W. Q. Tao, Field Synergy Principle and Its Applications in Enhancing Convective Heat Transfer and Improving Performance of Pulse Tube Refrigerators (Part 2), *J. Xi'an Jiaotong Univ.*, vol. 36, no. 11, pp. 1106–1110, 2002.
20. W. M. Kays and M. E. Crawford, *Convective Heat and Mass Transfer*, McGraw-Hill, pp. 107, 246, New York, 1980.
21. W. Q. Tao, *Numerical Heat Transfer*, 2d ed., Xi'an Jiaotong University Press, Xi'an, China, 2001.
22. S. V. Patankar, *Numerical Heat Transfer and Fluid Flow*, McGraw-Hill, New York, 1980.
23. W. Q. Tao, Recent Advances in Computational Heat Transfer, Science Press, Beijing, China, 2000.
24. Z. Y. Li and W. Q. Tao, A New Stability-Guaranteed Second-Order Difference Scheme, *Numer. Heat Transfer*, vol. 42, no. 4, pp. 349–365, 2002.
25. W. Q. Tao, Z. G. Qu, and Y. L. He, A Novel Segregated Algorithm for Incompressible Fluid Flow and Heat Transfer Problems—CLEAR (*C*oupled & *L*inked *E*quations

*A*lgorithm *R*evised) Part I: Mathematical Formulation and Solution Procedure, *Numer. Heat Transfer B*, vol. 45, pp. 1–18, 2004.

26. W. Q. Tao, Z. G. Qu, and Y. L. He, A Novel Segregated Algorithm for Incompressible Fluid Flow and Heat Transfer Problems—CLEAR (*C*oupled & *L*inked *E*quations *A*lgorithm *R*evised): Part II: Application Examples, *Numer. Heat Transfer B*, vol. 45, pp. 19–48, 2004.
27. C. C. Wang, K. Y. Chi, and C. J. Chang, Heat Transfer and Friction Characteristics of Plain Fin-and-Tube Heat Exchangers, Part II: Correlation, *Int. J. Heat Mass Transfer*, vol. 43, pp. 2693–2700, 2000.
28. R. K. Shah, Compact Heat Exchanger Surface Selection Methods, *Proc. Sixth Int. Heat Transfer Conf.*, Toronto, Canada, vol. 4, pp. 193–199, 1978.
29. B. Yu, J. H. Nie, Q. W. Wang, and W. Q. Tao, Experimental Study on the Pressure Drop and Heat Transfer Characteristics of Tubes with Internal Wavy-like Longitudinal Fins, *Heat Mass Transfer*, vol. 35, pp. 65–73, 1999.